MECHANISMS OF FISSION NEUTRON EMISSION

H. Märten

Technische Universität Dresden, Institut für Kern- und Atomphysik
Mommsenstrasse 13, D-O-8027 Dresden, Germany

Abstract: The time evolution in fission is the starting point for discussing not only the main mechanism of fission neutron emission, the evaporation from fully accelerated fragments, but also possible secondary ones connected with dynamical features of nuclear fission. "Asymptotic" conditions as relevant for describing the particle release from highly excited, rapidly moving fragments are defined. Corresponding statistical model approaches to fission neutron emission, based on the adequate consideration of the intricate fragment occurrence probability, reproduce most of the experimental data. The remarkable influence of fission modes on neutron observables is analyzed in the framework of a macroscopic-microscopic scission point model consistent with energy conservation. Finally, chances and deficiencies for solving the mechanism puzzle are summarized.

1. INTRODUCTION

The release of neutrons in nuclear fission is strongly connected with the excitation of single-particle degrees of freedom in large-scale collective nuclear motions. Nuclear fission as a total rearrangement reaction of a quantummechanical many-body system is incompletely understood. Theoretical treatments as comprehensively reviewed by Moreau et al. /1/ reflect many capabilities for the qualitative and partially semi-quantitative description of most of the fission observables, but indicate also the present deficiencies. A brief characterization of the time evolution in fission related to particle emission is given in Section 2.

Experimental together with theoretical studies already reviewed elsewhere /2,3/ provided the basic understanding of neutron emission in fission. Accordingly, most of the fission neutrons are evaporated from fully accelerated fragments. However, the role of secondary mechanisms is still unclear. Several works in this field yielded contradictory results. Whereas complex statistical-model approaches (SMA) based on the evaporation theory (Weisskopf relation /4/) or the statistical theory of nuclear reactions (Hauser-Feshbach theory /5/), but accounting for the intricate fragment occurrence probability P depending on mass (A)

and charge (Z) number, total kinetic energy (TKE), excitation energy E^*, and angular momentum J, is suitable to reproduce most of fission neutron observables (Section 3), approaches to secondary fission neutron emission are qualitative and yield only estimations of their characteristics (Section 4). The solution of this mechanism problem requires full-scale SMA calculations in comparison with complex experimental distributions to be obtained in multiparameter experiments involving fragment detection in combination with the spectroscopy of all fragment de-excitation products (neutrons and γ-rays mainly). Previous analysis procedures are discussed critically in Section 5.

In the case of sufficiently high incident energy multiple chance fission and, consequently, pre-fission neutron emission occurs. The competition between the particle and γ-ray emission channels as well as the fission channel was analyzed in the framework of a modified Hauser-Feshbach theory including pre-equilibrium emission /6,7/ and within the evaporation theory /8/. Recently the statistical multistep reaction theory has been extended to account for the fission channel in a simple approximation /9/. In particular, pre-fission neutron emission includes direct and pre-equilibrium contributions to be discussed in Section 6.

2. TIME EVOLUTION IN FISSION

2.1. From saddle to scission point

An actinide nucleus undergoing fission is characterized by the variables A_{FN}, Z_{FN}, E^*_{FN}, J_{FN}, and projection quantum number K_{FN} (FN - fissioning nucleus). These quantities define its fissility (Z^2_{FN}/A_{FN}), the fission probability (mainly via E^*_{FN}), the angular distribution of fission fragments (depending on J_{FN} and K_{FN}) and the occurrence probability $P(A,Z,TKE,E^*,J)$. Besides the influence of the transition states /10/ at both saddle points, the probability function P is mainly formed during the descent from the outside saddle point to the scission point. Whereas the potential energy at all deformation stages can be approximated by selfconsistent Hartree-Fock calculations /11/ or the macroscopic-microscopic method /12/, the time evolution of the fissioning nucleus and all its dynamic features, which is strongly related to nuclear inertia and dissipation, is still one of the

most challenging topics in the field. Both time-dependent (microscopic) Hartree-Fock (TDHF) calculations /13/ and macroscopic approaches (based on surface-plus-window dissipation or stochastic forces diffusing the dynamical paths in phase space or any other) to fission dynamics /14,15/ have led to quite different pictures. According to various dynamical calculations /16-19/, which differ in regard to dissipation mechanism, the transition time between saddle and scission point is in the order of (2 - 6) 10^{-21} s. Extreme estimates /17/ ranges up to 1.3 10^{-20} s.

Phenomenologically, one can assume that the potential energy gain between saddle and scission point is the sum of a dissipative energy E_{dis} and the kinetic energy of collective degrees of freedom, whose translational part appears as pre-scission kinetic energy of the fragments E_{pre}. The first term give rise to a scission point temperature τ_{sc} influencing the microscopic terms of the potential energy. The definition of a scission point is crucial, since it is not defined by static conditions alone, but can be understood as random neck rupture /20/, since the rather small transition time for the descent from saddle to scission point hiddens the fissioning system to reach equilibrium at scission point. Scission itselfes corresponds to a rapid change of nuclear potential. Strong single particle excitations and, consequently, particle emission at scission seem to be possible (cf. Section 4.1).

For simplicity, it is, however, useful to formulate a phenomenological energy balance equation for the scission point (in the present version without the indication of the explicite dependence on mass and charge asymmetry, on deformation variables and τ_{sc})

$$Q + E^*_{FN} = \underbrace{E_{pre} + E_{coul}}_{TKE} + \overbrace{\underbrace{\sum_i E_{def}(i)}_{F} + \underbrace{E_{dis} + E^*_B}_{E^*_{sc}}}^{\sum_i E^*(i)} , \qquad (1)$$

where Q is the total energy release for the given fragmentation $(A_1/A_2;Z_1/Z_2)$. The total intrinsic excitation energy E^*_{sc} at

scission is assumed as sum of E_{dis} and the excitation energy E_B^* at the second saddle. The variable F is the potential energy at scission, whose two parts, the Coulomb potential energy E_{coul} and the deformation energies $E_{def}(i)$ of the individual fragments (i), depend on the deformation (represented by a set of parameters). Eq. (1) together with the assumption of minimum F at scission may be used to deduce approximative scission point conditions defining the partition of the total available energy on both fragments /21/.

2.2. Post-scission dynamics

Besides the acceleration of the fragments in the Coulomb field starting with the initial condition E_{pre} at scission and resulting in TKE, the deformation energy dissipates into intrinsic excitation energy of the individual fragments. According to Eq. (1), $E^*(i)$ is additionally defined by a certain part of E_{sc}^*. This fraction may be calculated by thermodynamic assumptions /21/. The time evolution of these simultaneous processes, which occur within about $3\ 10^{-20}$ s after scission mainly /22/, is not well understood. At the beginning of the post-scission dissipation, which immediately follows the descent from saddle to scission point with the relevant dissipation, states far from equilibrium conditions are shortly occupied. Accordingly, non-equilibrium particle emission should be expected (cf. Section IV.2). In respect to neutron emission during fragment acceleration, the time evolution of the internal fragment dynamics is of high importance. That is, since the neutron emission time (corresponding to a certain fragment kinetic energy) defines emission kinetics and, therefore, the angular correlations between neutron and fragment.

2.3. "Asymptotic" conditions

Due to the dynamic processes discussed above, the probability function P depends on time. However, it is useful to define "asymptotic" conditions achieved after fragment acceleration (effectively finished at about $3\ 10^{-20}$s after scission) as well as dissipation of E_{def} into intrinsic excitation energy distributed among the single particle degrees of freedom according to equilibrium. These conditions hold before any de-excitation process. Hence, we have

$$TKE = E_{pre} + E_{coul}, \quad (2)$$

$$E^*(i) = E_{def}(i) + f(i)\, E^*_{sc}, \quad (3)$$

where f(i) is the fraction of scission point excitation energy coming to fragment (i). In regard to the probability function $P(A,Z,TKE,E^*,J)$, it is emphasized that for a given nucleon number partition $(A_1/A_2;Z_1/Z_2)$ resulting in a defined Q value, a distribution in TKE and E^* appears, where the constraint

$$Q + E^*_{FN} = TKE + \sum_i E^*(i) \quad (4)$$

must be met. For fixed $(A_1/A_2;Z_1/Z_2)$ and TKE, the ratio $E^*(1)/E^*(2)$ is distributed around an average value due to phase space conditions /23,24/. Obviously, the "asymptotic" distribution $P(A,Z,TKE,E^*,J)$ is the starting point for a SMA to neutron evaporation from fully accelerated fragments.

3. NEUTRON EVAPORATION FROM FULLY ACCELERATED FRAGMENTS

3.1. Experimental informations

Fission neutron emission was already found and roughly explained in 1939, i.e. a short time after the discovery of nuclear fission (Ref. /25/ and references therein). Stimulated by urgent nuclear data needs, prompt fission neutron spectra were measured for various nuclei in the early years of nuclear technology. They were successfully described in the framework of rather simple evaporation models assuming emission from fully accelerated fragments /26-28/. First measurements of angular correlations between fission fragments and neutrons confirmed the above assumption of the main emission mechanism. Based on Bohr's and Wheeler's hypotheses, that "hydrodynamical" distortions at the scission point should cause a further component, i.e. the so-called scission neutrons, several groups performed more sophisticated experiments started in the sixties /29-33/ and continued until the present time /34-52/. Such measurements provided data on yields, energy and angular distributions of fission neutrons in correlation with fragment parameters (A,TKE). In spite of some different, sometimes contradictory conclusions,

the most important result of all these works was the verification of neutron evaporation from fully accelerated fragments as the main emission mechanism. For secondary mechanisms and problems related to the analysis of experimental data, see Sections 4 - 5.

3.2. Statistical-model analysis

The adequate theoretical description of fission neutron emission should involve the complex fragment occurrence probability $P(A,Z,TKE,E^*,J)$ in order to account for the diversity of fragment configurations. Neglecting all secondary mechanisms, i.e. considering "asymptotic" conditions as discussed above, the standard statistical theory of de-excitation of highly excited nuclei can be applied to calculate fission neutron characteristics [multiplicity distributions $P(\nu)$ with the average neutron yield $\bar{\nu}$, double-differential distributions $N(E,\theta)$ in emission energy E and angle θ with reference to light-fragment direction, energy spectra N(E), as well as their correlation to fragment parameters]. Such a SMA can be based on the scheme represented below. Here, the "asymptotic" fragment distribution $P(A,Z,TKE,E^*,J)$ is splitted into $P(E^*,J:A,Z,TKE)$ for fixed A, Z, and TKE and $P(A,Z,TKE)$. Note that cascade emission in steps (i) of different particles π and γ-rays is considered. The centre-of-mass (CMS) spectrum $\varphi_\pi(\varepsilon_\pi)$ is represented by the spectral emission width $\Gamma_\pi(\varepsilon_\pi:E^*,J)$ according to the Hauser-Feshbach theory /5/:

$$\varphi_\pi(\varepsilon_\pi) = \sum_i \int dE^* \sum_J P_i(E^*,J) \frac{\Gamma_\pi(\varepsilon_\pi,E^*,J)}{\sum_{\pi''} \Gamma^{tot}_{\pi''}(E^*,J) + \Gamma^{tot}_{\gamma}(E^*,J)}, \quad (5)$$

$$\Gamma_\pi(\varepsilon_\pi,E^*,J) = (2\pi\,\rho(E^*,J))^{-1} \sum_{J'} \rho^\pi(U_\pi,J') \sum_{l_\pi,j_\pi} T^\pi_{lj}(\varepsilon_\pi), \quad (6)$$

where ρ is the level density, and T_{lj} is the transmission coefficient for angular momentum l and channel spin j ($\vec{j} = \vec{l} + \vec{s}$) with s as the particle spin. Excitation energy U and spin J′ of the rest nucleus after particle emission is given by

$$U_\pi = E^* - B_\pi - \varepsilon_\pi, \text{ and } \vec{J} = \vec{J}' + \vec{l}_\pi + \vec{s}_\pi, \quad (7)$$

respectively (B_π - separation energy of particle π). Starting with

the initial distribution $P_{i=0}(E^*,J)$, all $P_i(E^*,J)$ for $i \geq 1$ are deduced from the distribution of the preceding emission step using (7). Considering CMS anisotropy due to fragment spin J (calculated either via the Legendre polynoms $P_l^2(\cos\vartheta)$ /53/ for given l or by a semi-classical approach /54/), one obtains the double differential probability $\varphi_\pi(\varepsilon_\pi,\vartheta_\pi:A,Z,TKE)$ in CMS, which has to be transformed into the corresponding laboratory system (LS) distribution $N_\pi(E,\theta:A,Z,TKE)$ on the basis of the kinematic relations

$$\varepsilon = E + E_f - 2\,(E\,E_f)^{1/2}\cos\theta, \qquad (8.1)$$

$$E = \varepsilon + E_f + 2\,(\varepsilon\,E_f)^{1/2}\cos\vartheta, \qquad (8.2)$$

$$N(E,\theta) = (E/\varepsilon)^{1/2}\,\varphi(\varepsilon,\vartheta). \qquad (9)$$

(E_f - fragment kinetic energy per nucleon).
Finally, the total LS emission probability is given by

$$N_\pi(E_\pi,\theta_\pi) = \sum_{A,Z} \int dTKE\; N_\pi(E,\theta:A,Z,TKE)\; P(A,Z,TKE). \qquad (10)$$

Besides $P(A,Z,TKE,E^*,J)$, which is - in most cases - not known with sufficient accuracy and/or complexity, <u>global</u> descriptions of nuclear level densities and transmission coefficients for neutron-rich fission fragments are necessary preconditions for full-scale calculations following the scheme outlined above.

Level densities: Budtz-Jorgensen and Knitter /51/ analyzed average level density parameters a(A) for fission fragments on the basis of experimental multiparameter data. As shown in Fig. 1, these data can be well described on the basis of a semi-empirical approach including microscopic effects (shell energy, pairing energy) /55/. In this calculation, ρ was deduced as function of average rest-nucleus excitation energy obtained from cascade evaporation calculations /23/ and for average pairing energies.

Optical potential: Various global parameterizations /56-59/ of the neutron optical potential were tested /3/ within fission neutron observables calculations. Fig. 2 represents the course of the compound-nucleus formation (inverse) cross section obtained

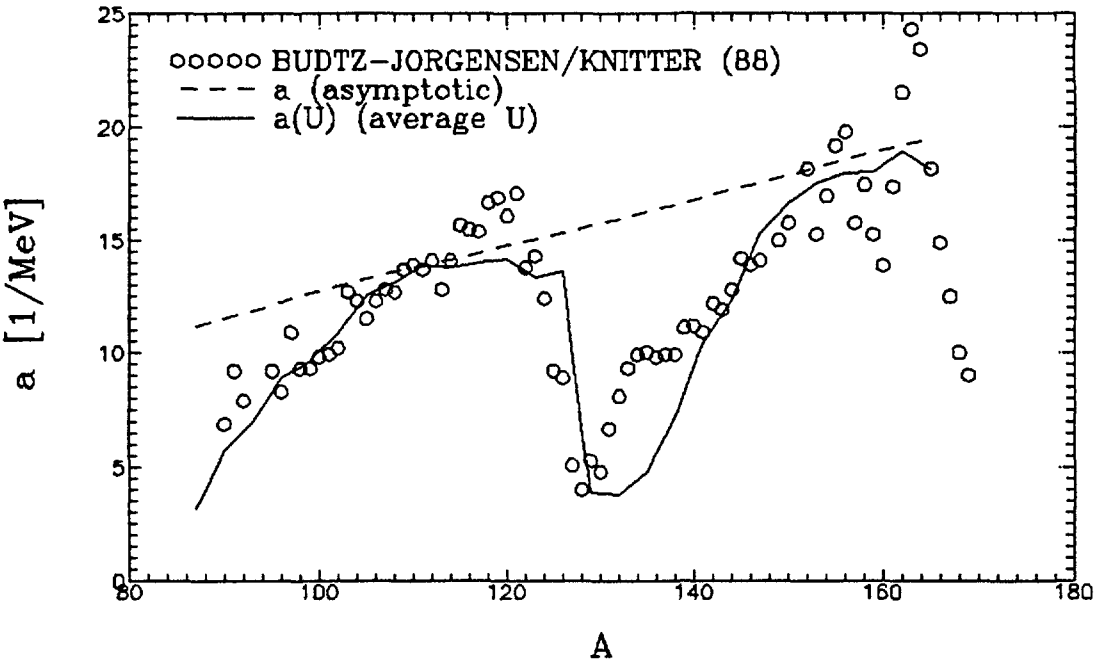

Fig. 1 Level density parameter (a) for neutron-rich fission fragments from ^{252}Cf(sf) (circles - /51/, solid line - calculation /55/ as function of average rest-nucleus energy /23/, dashed line - asymptotic value, i.e. for vanishing microscopic energies)

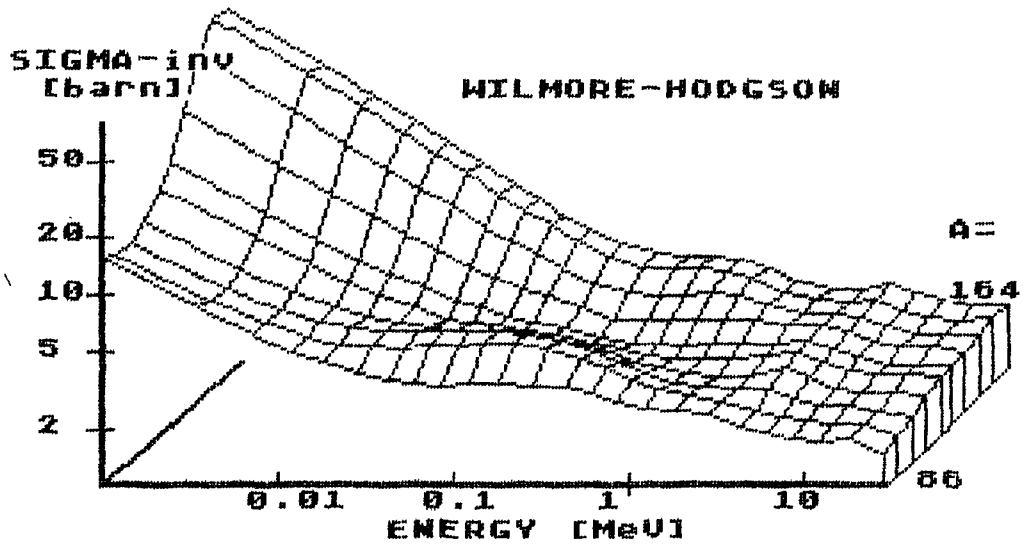

Fig. 2 Compound-nucleus formation cross section for neutron-rich fission fragments (global optical potential taken from Ref. /58/)

for fission fragments in the 87 - 165 mass number range. Note the remarkable mass number dependence at low energy, which is of importance in understanding differences in differential neutron characteristics between light and heavy fragments, e.g. at CMS energies $\varepsilon \rightarrow 0$, i.e. for $E \rightarrow E_f$ and $\theta \rightarrow 0$. Within the global optical potential parameterization, the consideration of the isospin dependence /57/ is very important for applications to

neutron-rich fission fragments. However, further uncertainty factors (range of applicability concerning energy range, mass number range, reaction channels etc.) do not automatically favour such types of potential parameterization against others.

As already summarized in /3/, the idealized SMA outlined above has to be simplified to make it tractable. In particular, the fragment occurrence distribution is not known in its full complexity (even in the most promising case of ^{252}Cf(sf)). Hence, simplifications concern the fragment distribution P(A,Z,TKE,E^*,J) by reducing it to average values of the fragment variables as well as the evaporation formalism. The following types of fission neutron models are used:

Hauser-Feshbach models /60-62/ including the spin dependence of neutron emission in competition to γ-ray and charged particle release (Eqs. 5-7).

Cascade evaporation models /23,28,52/ based on the Weisskopf formula, i.e. neglection of spin effects on emission spectra.

Temperature distribution models /8,63/ assuming a distribution in rest-nucleus temperature instead of a fragment distribution in E^*.

Statistical Multistep Compound Theory /52/ based on master equation approach simulating dissipation after scission point and accounting for possible non-equilibrium effects (cf. Section 4.2).

Any other, more rough models not discussed here.

Besides the fundamental ansatz to describe the emission spectrum for given A, Z, E^* (and J), the account for P(A,Z,TKE,E^*,J) to more or less extent gives the possibility to distinguish between different models.

The Figs. 3-6 represent some examples of calculational results reproducing experimental data on energy spectra N(E) and double-differential emission distributions N(E,θ) for ^{252}Cf(sf). The calculations were performed in the framework of either the Hauser-Feshbach model /62/ or the cascade evaporation (Weisskopf) model /23,52/ for a rather complex fragment distribution P(A,TKE,E^*) with $\bar{Z}$(A) and $\bar{J}$(A).

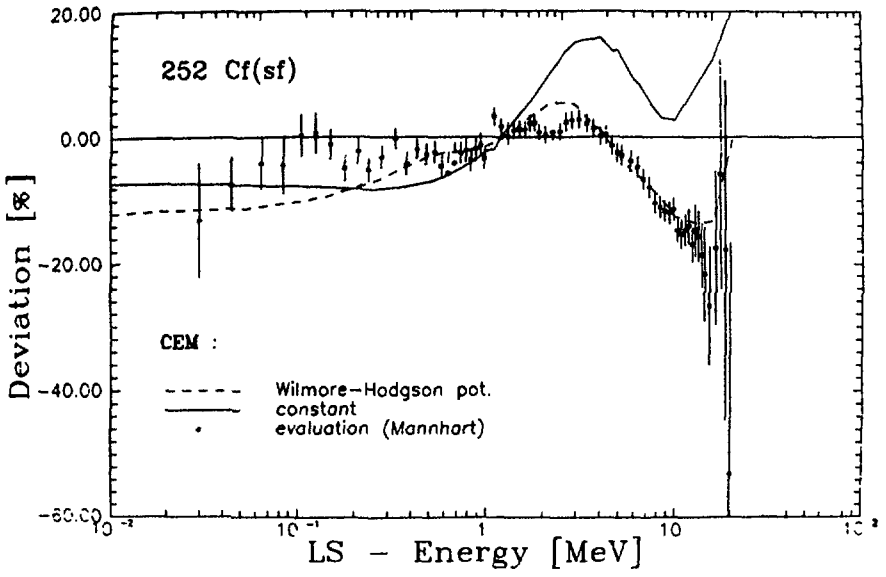

Fig. 3 The energy spectrum of neutrons from ^{252}Cf(sf) represented as percentage deviation D from a reference Maxwellian distribution with a "temperature" parameter T = 1.42 MeV (dots - evaluation /64/, lines - cascade evaporation calculation for global optical potential taken from /58/ as well as for constant inverse cross section of compound nucleus formation)

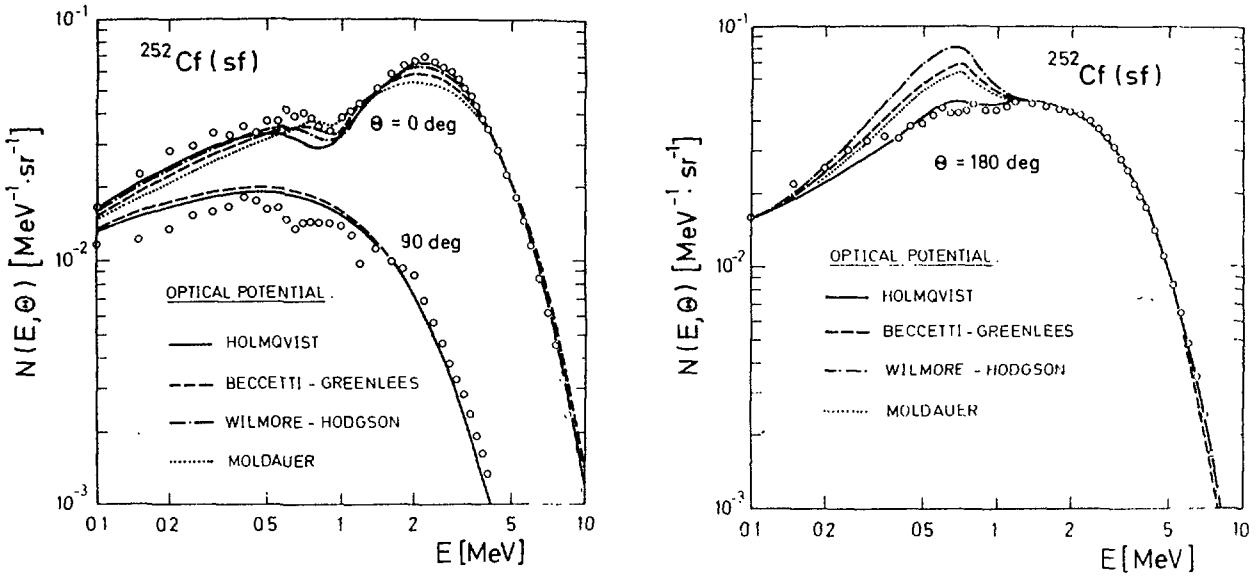

Fig. 4 Differential neutron spectra of ^{252}Cf(sf) neutrons at θ = 0 and 90 deg (left) and θ = 180 deg (right) (circles - experimental data /65/, lines - cascade evaporation calculation for several global optical potentials /56-59/ as indicated)

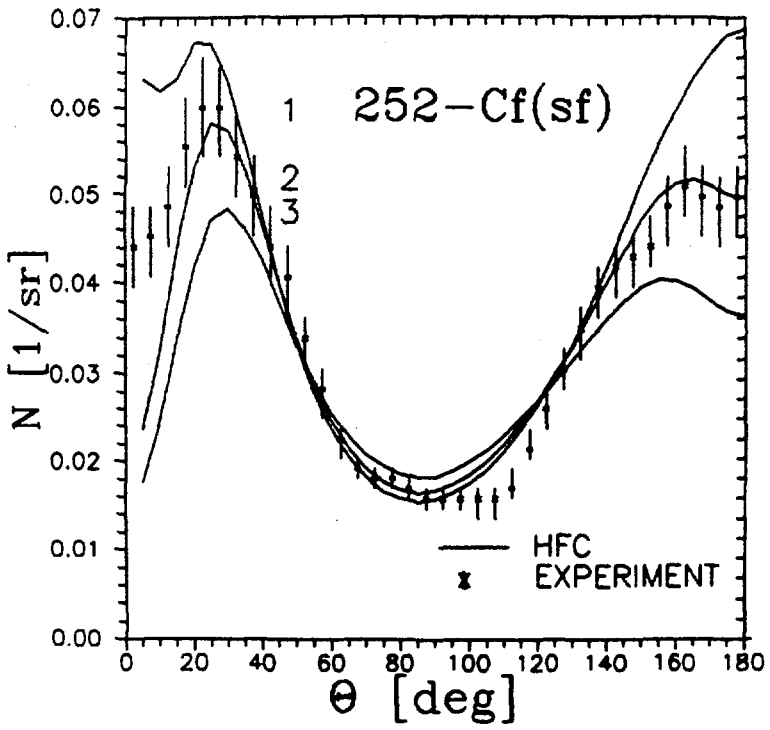

Fig. 5 Angular distribution of ^{252}Cf(sf) neutrons at E = 1 MeV (dots - experimental data /65/, lines - Hauser-Feshbach calculation for different choices of γ-ray emission width description /62/)

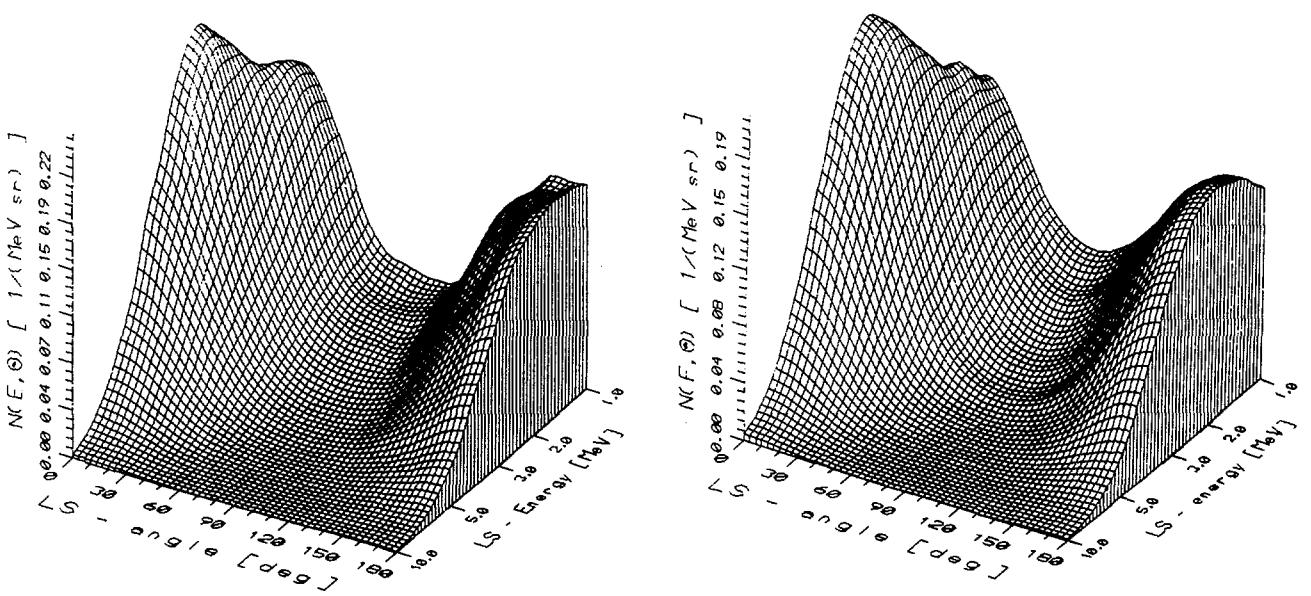

Fig. 6 Plot of the double differential distribution of ^{252}Cf(sf) neutron emission N(E,θ) (left - experimental data /65/, right - cascade evaporation calculation /52/)

The CMS neutron spectra are commonly fitted to the ansatz

$$\varphi(\varepsilon) = [\ T^{\lambda+1}\ \Gamma(\lambda+1)\ ]^{-1}\ \varepsilon^{\lambda}\ \exp(-\varepsilon/T) \qquad (10)$$

including the "hardness" or "temperature" parameter T and the "shape" parameter λ.

As discussed elsewhere /66/, λ as relevant for low CMS energy defines the course of the LS $N(E,\theta)$ distribution for $E \to E_f$ and $\theta \to 0$ (i.e. $\varepsilon \to 0$, cf. (8) and (9)). The cascade evaporation model reproduces fairly well the data deduced from experiment /51/. Note that (due to the rough approximation of the spectral shape by (10)) the parameter λ deduced from the whole spectrum differs from the value λ obtained by fitting the low-energy spectrum part. Whereas the first one is determined by the level density description and $P(E^*)$, the second one depends on optical potential, the degree of cascade emission, and the strength of γ-ray emission at E^* above neutron separation energy. The Figs. 7-9 represent calculational data in comparison with experimental ones.

The agreement between experimental data and SMA calculations confirms the assumption that (at least most of) fission neutrons are evaporated from fully accelerated fragments. However, the

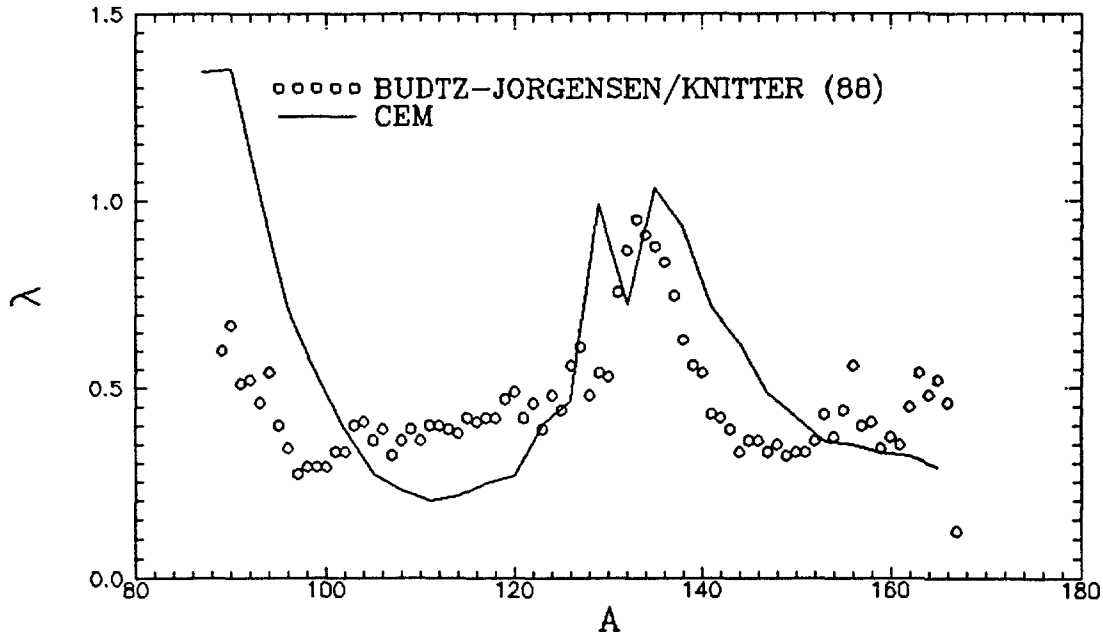

Fig. 7 CMS spectral "shape" parameter λ for $^{252}Cf(sf)$ neutron emission (dots - experimental data /51/, line - cascade evaporation calculation /66/)

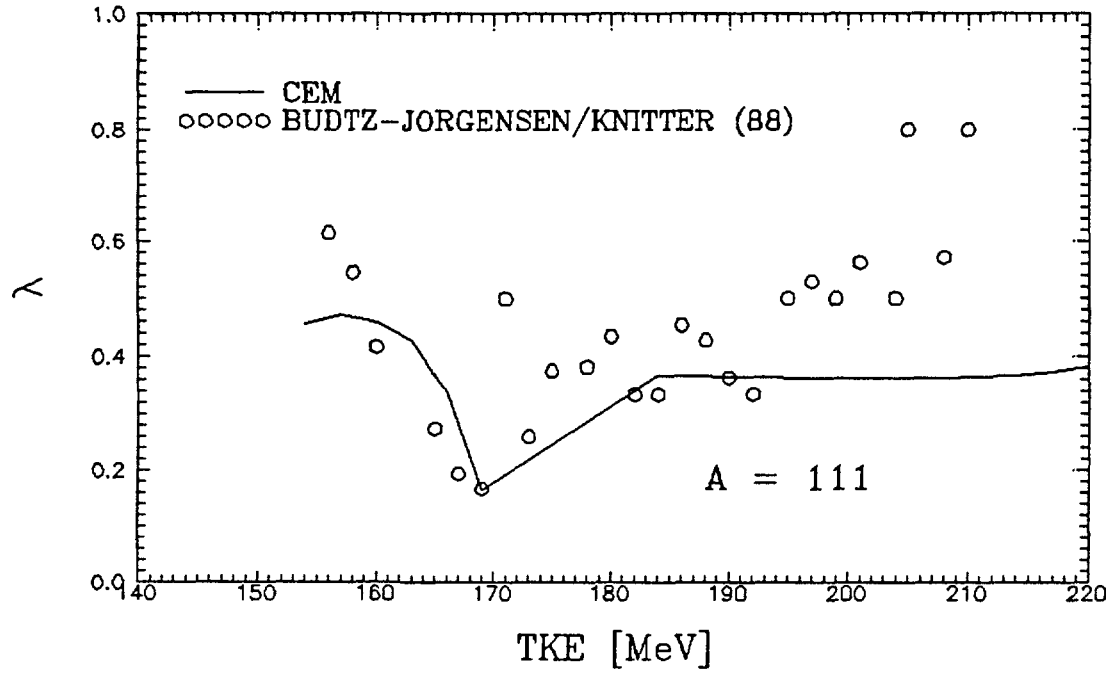

Fig. 8 The same as for Fig. 7, but for fixed A = 111 and in dependence on TKE

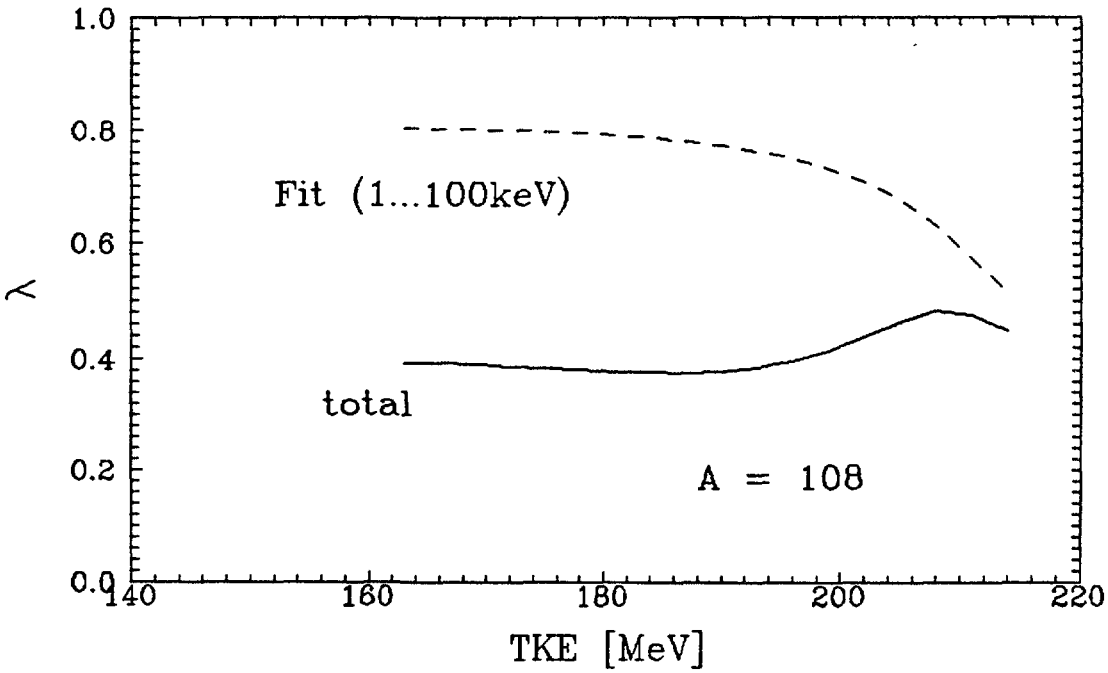

Fig. 9 Spectral "shape" parameter λ deduced from the total CMS 252-Cf(sf) neutron spectrum on the one side and fitted to the low-energy region (1 - 100 keV) on the other side (cascade evaporation calculation). Note that $\lambda > 0.5$ (as obtained for low emission energy) causes a dip in the $N(E,\theta)$ distribution at $E \rightarrow E_f$ and $\theta \rightarrow 0$ (cf. Fig. 6).

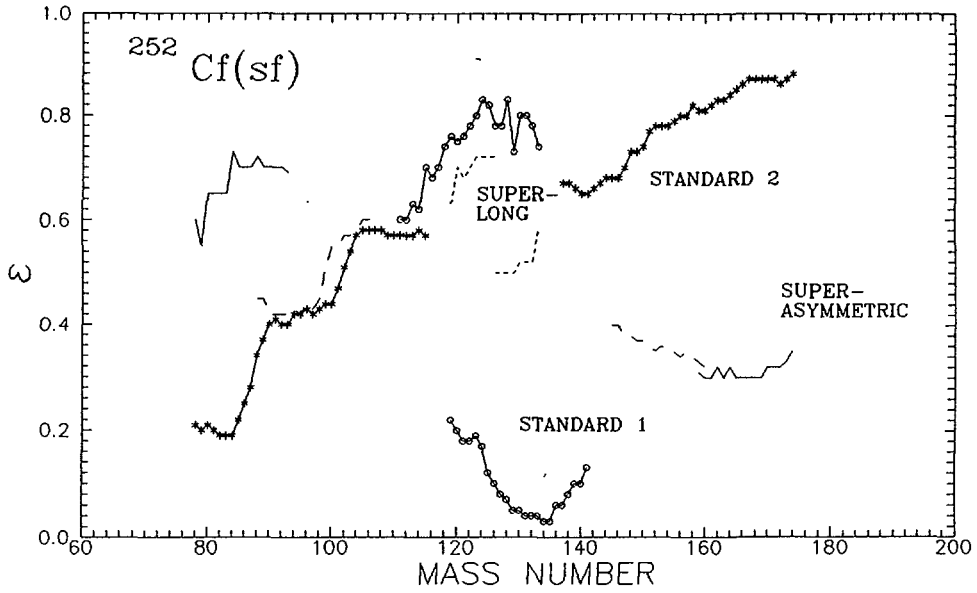

Fig 10 Position of the extrema in the scission point potential energy surface as function of individual fragment deformation ε. These extrema correspond to the so-called fission modes. The denotation corresponds to that one of Brosa /68/.

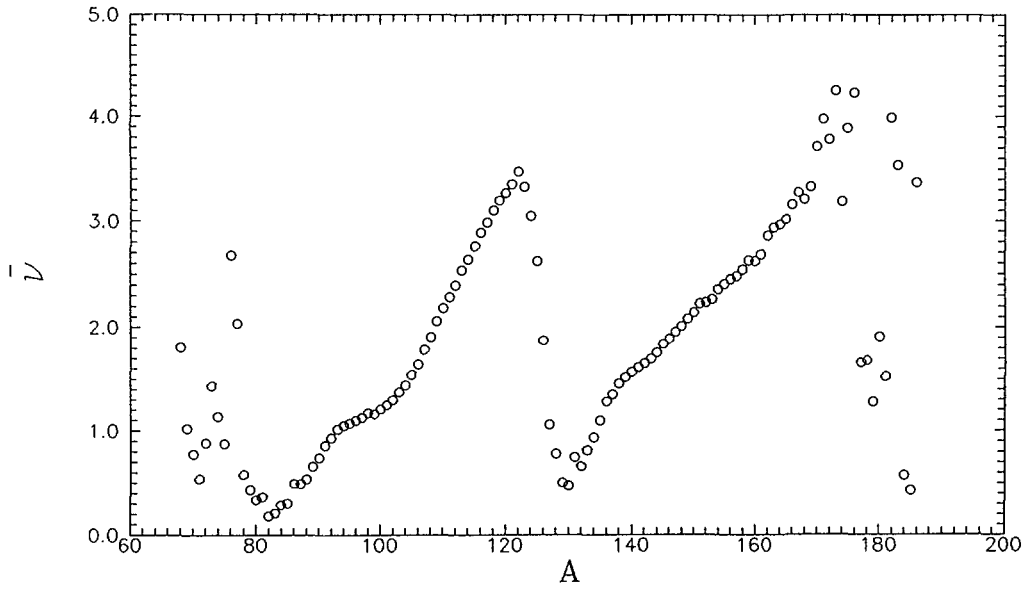

Fig. 11 Average neutron multiplicity versus fragment mass number for 252-Cf(sf) (dots - experimental data /51/). The abbreviations indicate the fission modes forming the triple saw-tooth (cf. Fig. 10).

calculational examples shown above were based on fragment occurrence distributions deduced from experimental data on fragment yields, neutron multiplicity distributions and fission γ-rays /23/. The prediction of P(...) on theoretical basis involves rather large uncertainties. Nevertheless, it can be used for qualitative studies as shown below.

3.3. Fission modes and their influence on neutron observables

The multimodal fission model by Brosa et al. /67/ predicts preferred fission channels (corresponding to paths, i.e. ridge lines, in potential energy surface covering the range from saddle to scission point). Their appearance is the reason for the saw-tooth like neutron multiplicity curve $\bar{\nu}(A)$ /68/. Already in the framework of a macroscopic-microscopic scission point model with account for energy balance (1) /21a/ fission modes may be deduced. They correspond to extrema in the potential energy surface in the deformation space close to scission point. Within the ε-parameterization /69/ of deformed fragments at scission, the positions of these extrema have been determined as function of individual fragment deformation ε at scission point. The result is represented in Fig. 10. Accordingly, average neutron multiplicity $\bar{\nu}(A)$ reflects the occurrence of the fission modes as function of mass asymmetry. In particular, the triple saw-tooth measured by Budtz-Jorgensen and Knitter /51/ can be explained (as already done by Brosa). Results are shown in Fig. 11.

Finally, we discuss the influence of fission modes on the distribution in E^* for A = 132, i.e. the nearly double-magic fragment. It arises in the standard 1 fission mode mainly. However, a competing fission channel for this mass split is standard 2. Fig. 12 represents the distribution $P(E^*)$ obtained in

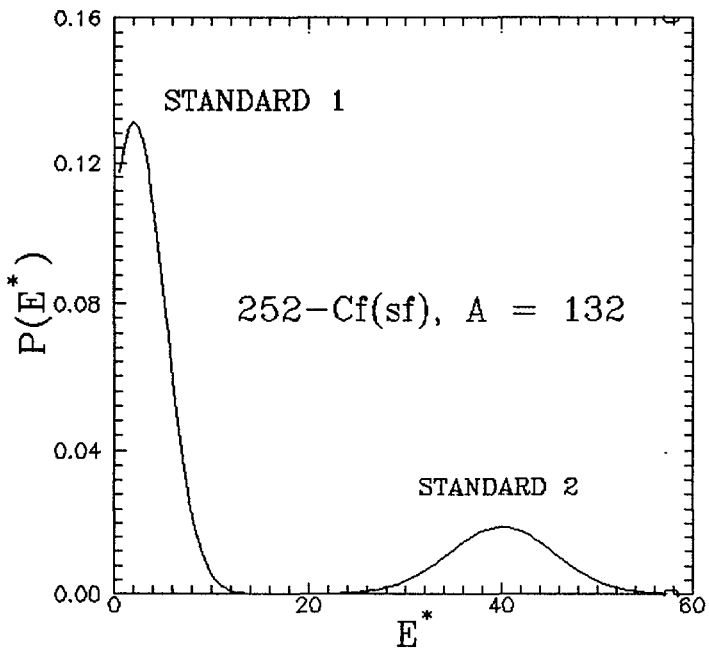

Fig. 12 Calculational distribution $P(E^*)$ for the fragment with A=132 from 252-Cf(sf)

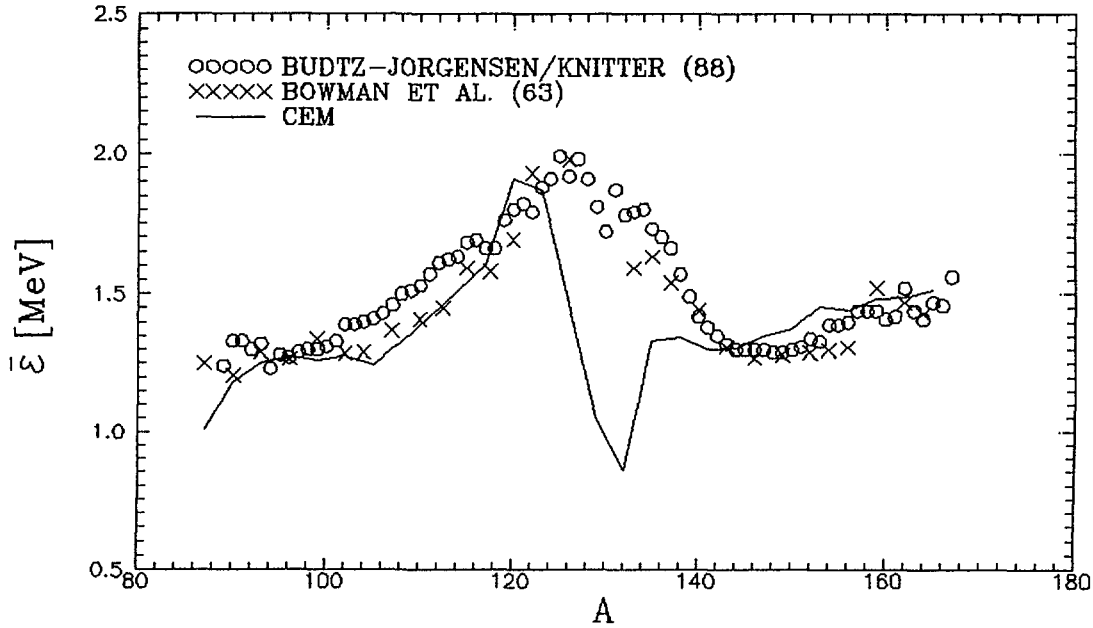

Fig. 13 Average CMS emission energy of neutrons from ^{252}Cf(sf) as function of fragment mass number (dots - /51/, crosses - /32/, line - cascade evaporation calculation)

the framework of the above scission point model. It shows a high-energy component due to standard 2. Its yield is strongly parameter dependent. It should be taken as an qualitative picture. However, this appearance gives a possible explanation of the old discrepancy between measured average CMS emission energies of neutrons from ^{252}Cf(sf) and evaporation calculations for A around 132 (Fig. 13).

4. "SECONDARY" MECHANISMS

The most challenging question in fission neutron mechanism studies concerns any deviations from the "normal" one, which are due to "non-asymptotic" conditions.

4.1. Scission neutrons

Started in the early sixties, several groups /32-36/ analyzed multiparameter data on fission neutron emission, e.g. angular inclusive or exclusive distributions, in order to derive informations about scission neutrons. The analysis procedures were commonly based on the assumption that

(i) scission neutrons are emitted isotropically in LS, and

(ii) simple evaporation ansatzes with parameters deduced from the experiment (!) describe the "normal" component due to statistical neutron emission from fully accelerated fragments.

In most cases, the enhancement of the θ=90 deg data (either yield or spectral distribution) with reference to the evaporation calculation was interpreted as due to scission neutrons. Their total yield was found in the range between 0 % /35/ and 25 % /37/. Further studies included the investigation of scission neutron yield as function of TKE. Here, an increase /43/, independence /37/ as well as decrease /42/ was found by different authors. Contradictory results were also published about the average emission energy of scission neutrons: 1.65 MeV /42/, 2.0 MeV /44/, 2.4 MeV /37/, and 2.6 MeV /32/ (for ^{252}Cf(sf)). More recent studies indicate that the scission neutron yield is very small (according to /70/, $\bar{\nu}_{sc}$ = (0.01 ± 0.003), i.e. about 0.27 %, with an average emission energy of 0.4 MeV for ^{252}Cf(sf)) or vanishing /50/ (estimation of a 5 % upper yield of secondary neutrons accounting for theoretical as well as experimental uncertainties). A brief evaluation of analysis procedures will be given in Section 5.

The theoretical understanding of particle emission close to scission point is still a challenging problem. After a more general discussion by Stavinsky /71/, Fuller /72/ was the first who studied the effect of single-particle excitation due to rapid changes of the nuclear potential during the descent from saddle to scission point. In /73/, calculations were performed for more realistic potentials. However, the strong dependence of the calculated particle yields on input parameters (e.g. time constants) do not allow for any definite conclusions about this mechanism. Rubchenya /74/ investigated single-particle excitations due to the snatching of a strongly deformed fragment just after scission. Consequently, scission neutrons are expected for scission configurations with high deformation of at least one fragment. Based on a similar picture, Mädler /75/ proposed the catapult mechanism and studied it within time-dependent Hartree-Fock calculations. The two-centre shell model connected with the assumption of an "activated" particle was the basis for the study by Milek et al. /76/. The angular distributions calculated in this

work are clearly not isotropic, but exhibit an interference structure. These results are in contradiction with the previous assumption that scission neutrons are an isotropic component /32/.

4.2. Neutron emission during fragment acceleration

The scission neutron mechanisms proposed by Rubchenya, Mädler, and Milek et al. must be classified into a time scale just after scission, i.e. these are, strictly speaking, part of neutron emission during fragment acceleration. In general, this component firstly discussed by Eismont /77/ and studied by Pik-Pitchak /78/ within a simple evaporation approach ("abrupt" dissipation limit) has to be separated from the main evaporation mechanism because of different kinematic conditions and other excitation states in the dissipating fragments. Earlier works were based on the assumption that the asymptotic excitation energy is already available at scission point /78,79/ (i.e. "abrupt" dissipation) and that neutrons are evaporated from thermal equilibrium. This gives rise to an enhancement of neutron emission in equatorial direction ($\theta \cong$ 90 deg). Considering the post-scission dynamics studied by Samanta et al. /80/, different versions of characteristic dissipation time scales were assumed in the framework of a time-dependent cascade evaporation model in /81/. It was shown that the influence of the neutron emission during fragment acceleration on the total distribution $N(E,\theta)$ is strongly dependent on the characteristic dissipation time. Within the "moderate" limit /80/ ("slow" dissipation), neutron emission is reduced at θ close to 90 deg because of the "weak" CMS spectra in the time range up to about $5\ 10^{-20}$ s after scission. The opposite effect appears assuming "abrupt" dissipation (as already discussed). Neutron evaporation during fragment acceleration is illustrated in the Figs. 14-16.

The figures show clearly that the emission component of neutrons appearing during fragment acceleration is strongly dependent on dissipation mechanism, which is, however, not well understood. Hence, the effect studied gives rise to principal theoretical uncertainties of fission neutron calculations and, consequently, of mechanism studies.

A statistical description of neutron emission during fragment acceleration within multistep reaction theory was firstly proposed in /52/. According to Eq. (3), the fragments at scission point are

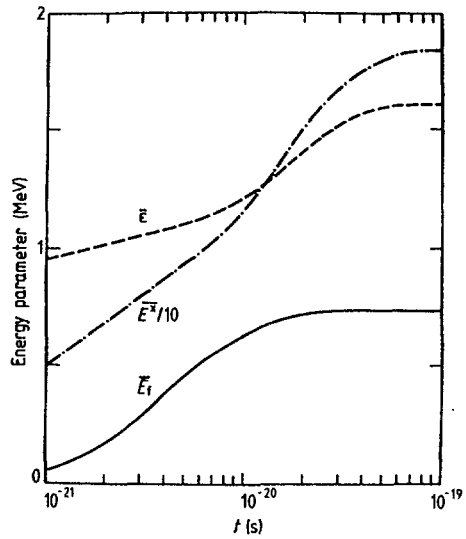

Fig. 14 Kinetic energy per nucleon and excitation energy of symmetric fragments from 252-Cf(sf) and average CMS energy of neutrons as function of time after scission /81/

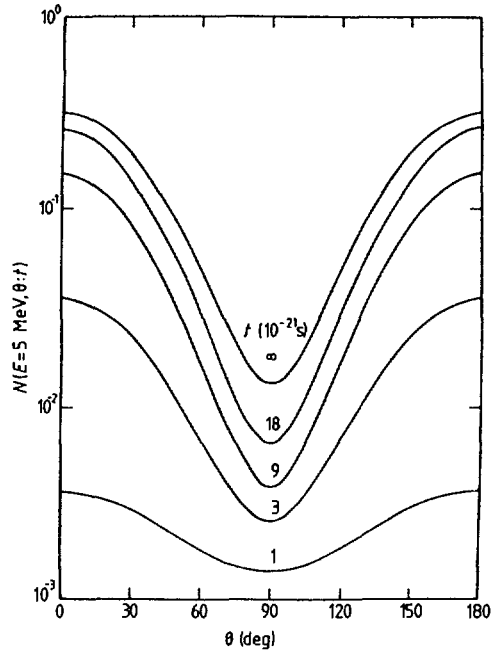

Fig. 15 Angular distribuzion of neutrons for fixed LS energy (E = 2 MeV) as function of t /81/

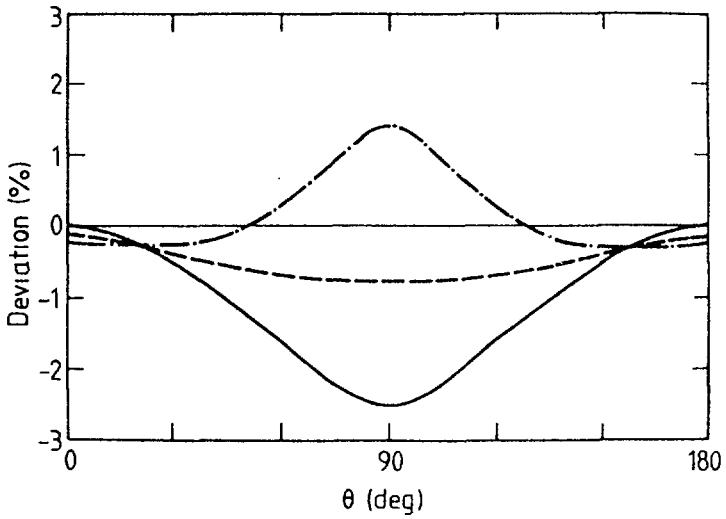

Fig. 16 Percentage deviation of the total angular distributions of E = 2 MeV neutrons from the "asymptotic" SMA calculation. Calculations were performed for "abrupt" (solid), "fast" (dashed), and "moderate" (dashed-dotted) dissipation /81/.

characterized by deformation energy $E_{def}(i)$ and a certain fraction f(i) of intrinsic excitation energy E^{*}_{sc} available at scission. In order to simulate an initial distribution $p_o(n)$ in exciton number n one may assume

$$p_o(n) = \alpha \, \delta_{nn_o} + (1 - \alpha) \, \delta_{n\bar{n}} \qquad (11)$$

with the initial exciton number (doorway state) n_o as the starting condition for dissipation of E_{def} into intrinsic excitation energy, and $\bar{n}$ as the average exciton number corresponding to the the fraction $f(i)E^*_{sc}$, which is assumed to be in thermal equilibrium. The fraction α is given by the ratio

$$\alpha = E_{def} / (E_{def} + f\, E^*_{sc}) = E_{def} / E^*. \qquad (12)$$

It can be deduced in the framework of an energy partition model (scission point model) with account for energy conservation as proposed in /63,82/. The statistical multistep reaction theory /83,84/ can be applied to the present problem. The statistical multistep compound part (SMC)

$$\rho^{SMC}(\varepsilon) \sim \sum_n \tau_n/h \left[\Gamma_n^{(o)\uparrow}(\varepsilon) + \Gamma_n^{(-)\uparrow}(\varepsilon) \right] \qquad (13)$$

as evident here is described on the basis of the master equation (in time-integrated form)

$$-\, h\, p_o(n) = \Gamma_{n-2}^{(+)\downarrow}(\varepsilon)\, \tau_{n-2} + \Gamma_{n+2}^{(-)\downarrow}(\varepsilon)\, \tau_{n+2} - \Gamma_n\, \tau_n \qquad (14)$$

leading to the average lifetime τ_n of the exciton state n. The damping width $\Gamma^{\downarrow}$ and the escape width $\Gamma^{\uparrow}$ enter the equations for exciton number changes $\Delta n = +2$, 0, and -2 corresponding to the superscripts (+), (0), and (-), respectively. The total width Γ_n is the sum of all damping and escape width. Within the closed-form SMC approach applied here, all matrix elements for bound-bound transitions I^2_{BB} cancel exactly in the sum of Eq. (13), since the matrix elements for bound-unbound transitions defining the escape widths are represented in terms of I^2_{BB}. Hence, the shape of the SMC spectrum is independent of I^2_{BB}, but is mainly determined by the single-particle state density. This SMC approach has successfully been verified (cf. applications to nuclear reactions up to energies of about 100 MeV /84/ together with the description of the statistical multistep direct part). The SMC approach to fission neutron emission was tested at first assuming the equilibrium limit (emission from fully accelerated fragments). An example is shown in Fig. 17.

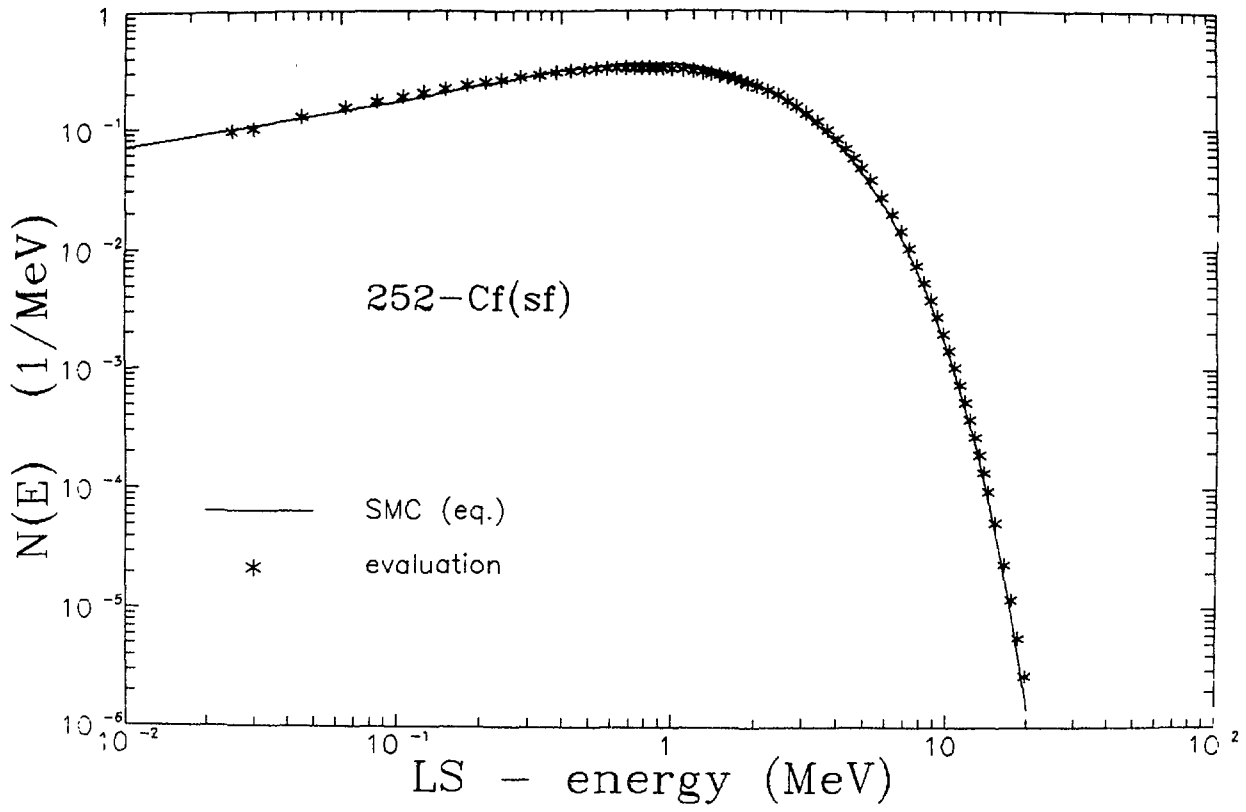

Fig. 17 SMC spectrum of ^{252}Cf(sf) neutrons (equilibrium limit) in comparison with Mannharts /64/ evaluation (taken from /52/)

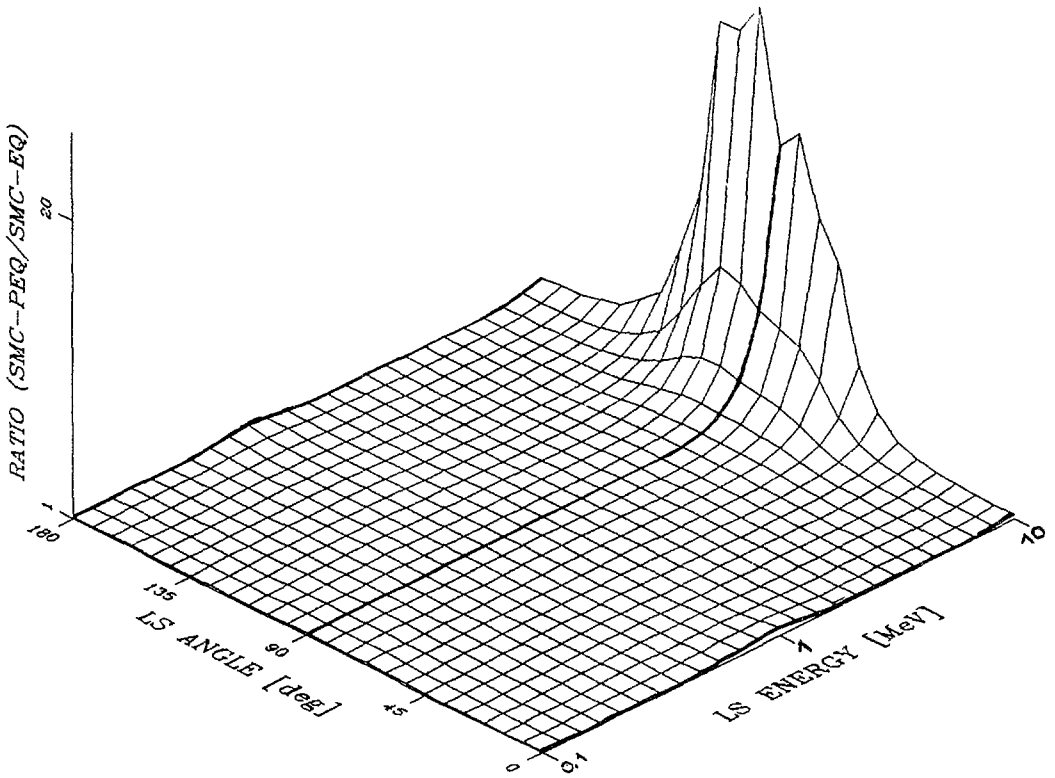

Fig. 18 Ratio of SMC to SMC(eq) calculation for ^{252}Cf(sf) in the LS variable field (E,θ)

The SMC results including preequilibrium emission during fragment acceleration, which were obtained with account for CMS-LS transformation as function of time after scission, do not significantly differ from the equilibrium limit SMC(eq) but in equatorial direction and at high energies. This fact is illustrated in Fig. 18. The LS variable region at θ close to 90 deg and at high emission energy is characterized by a very low emission probability, where experimental data exhibit rather large uncertainties. Recent measurements /50,51,85/ indicate that a preequilibrium component is probably existing. However, a clear confirmation of this effect is still open.

4.3. Neutrons from ^{5}He-decay after ternary fission events

Neutron release in nuclear fission after the decay of ^{5}He nuclei was studied by Cheifetz et al. /86/. However, ternary fission events with ^{5}He production is very rare. About 11 % of α particles from ^{252}Cf(sf) fission are originally released as n-unstable ^{5}He nuclei which decay with a halflife of about 8 10^{-22} s /86/. Calculations were performed /2/ assuming isotropic decay in CMS, a time-dependent distribution of ^{5}He kinetic energy, and an angular distribution of ^{5}He nuclei with reference to fission axis as for ^{4}He. The result is shown in Fig. 19. As to be expected, the angular distribution is pronounced at equatorial direction. The course of the 1 MeV angular distribution is caused by kinematic effects.

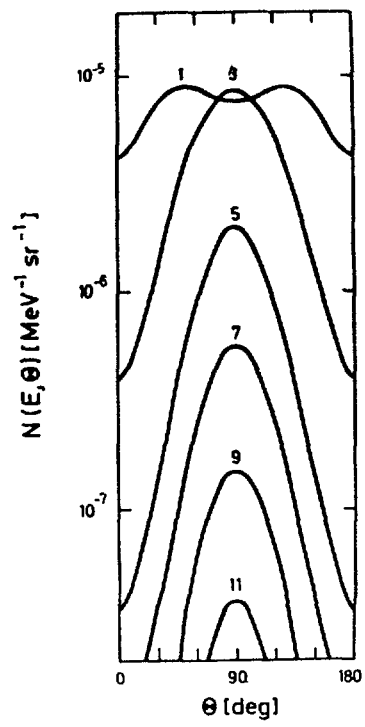

Fig. 19 Calculated angular distribution of neutrons from 5-He decay (parameter - LS energy [MeV])

Comparing these results with the total distribution of fission neutrons one can see that this component is less important.

5. THE MECHANISM PUZZLE - CHANCES AND DEFICIENCIES

In summary, it is emphasized that mechanisms of neutron emission in low-energy fission other than evaporation *from* fully accelerated fragments are really secondary. Deviations of differential (exclusive) experimental data from SMA predictions are commonly a consequence of non-adequate assumptions concerning the fragment distribution P (in particular, drastic variable averaging), sometimes neglection of fission mode influences as discussed above and rough CMS spectrum approximations. Only after clarifying these circumstances, one should draw definite conclusions about any secondary mechanisms. The derivation of CMS spectrum parameters from experimental data and the application of such (rough) spectrum ansatzes to describe differential LS emission probabilities as done in several previous works must be evaluated as at least crucial. Chances to get more informations about fission neutron mechanisms should be seen in combining further precise exclusive measurements of multiparameter fission neutron data with detailed theoretical descriptions on the basis of full-scale fragment distributions as discussed in this work.

6. MULTIPLE-CHANCE FISSION

At neutron incident energy above about 6 MeV, multiple chance fission reactions (n,xnf) appear in neutron induced reactions of actinide nuclei. The neutrons emitted before, but in coincidence with fission are called pre-fission neutrons. Their emission mechanisms are identical to those known from nuclear reaction studies. Besides equilibrium emission described by the use of statistical methods (Hauser-Feshbach, Weisskopf-Ewing, or any other), pre-equilibrium emission and direct processes appear. From the energetic point of view, the only one condition for a multiple chance fission is the constraint that the rest excitation energy after one (or more) neutron emissions is above the fission barrier B_f. The partial fission cross sections together with the pre-fission neutron spectra were described within the evaporation limit /8/ or by using Hauser-Feshbach theory extended by a pre-

equilibrium description /6,7/ (code STAPRE). Recently, Polster /9/ proposed a method for including the fission channel in the statistical multistep reaction theory of Kalka /84/. Here, fission is a further competing channel within SMC. The exciton-number dependent fission escape widths were deduced on the basis of statistical arguments:

$$\Gamma^{\uparrow}_{nf}(E^{*}_{FN},E') = \rho_n(E^{*}_{FN}-B_f-E') \;/\; [\; 2\pi\; \rho_n(E^{*}_{FN})\;] \qquad (15)$$

with E′ as the energy of the collective fission degree of freedom. Here, E^{*}_{FN} is the excitation energy of the actinide compound system decaying either by particle (neutron) emission, γ-ray emission or fission. Results are presented for neutron induced fission of ^{238}U in Fig. 20 and 21.

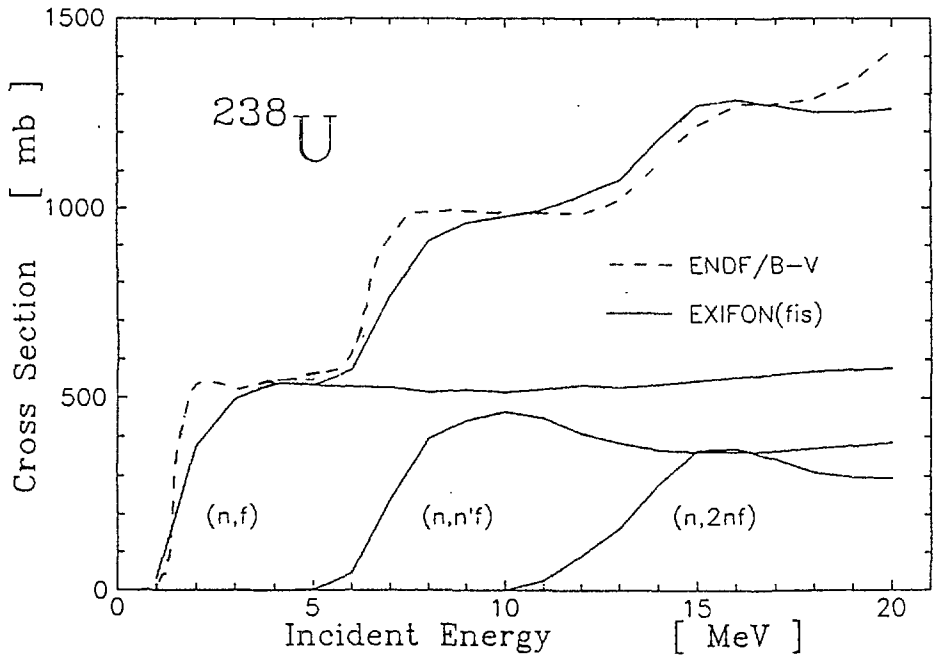

Fig. 20 Fission cross section for ^{238}U(n,xnf). Calculated results obtained within statistical multistep reaction theory extended by the fission channel are compared with ENDF/B-V data.

The fission neutron spectrum for ^{238}U + n (14.7 MeV) consists of three partial post-fission neutron spectra calculated by the use of FINESSE /63/ (on the basis of an macroscopic-microscopic energy partition model including mass asymmetry dependence) as well as the pre-fission neutron spectra from the (n,nf) and the (n,2nf) reaction obtained within EXIFON (statistical multistep reaction theory code /84/) extended by the fission channel. The calculated data are in good agreement with measured results.

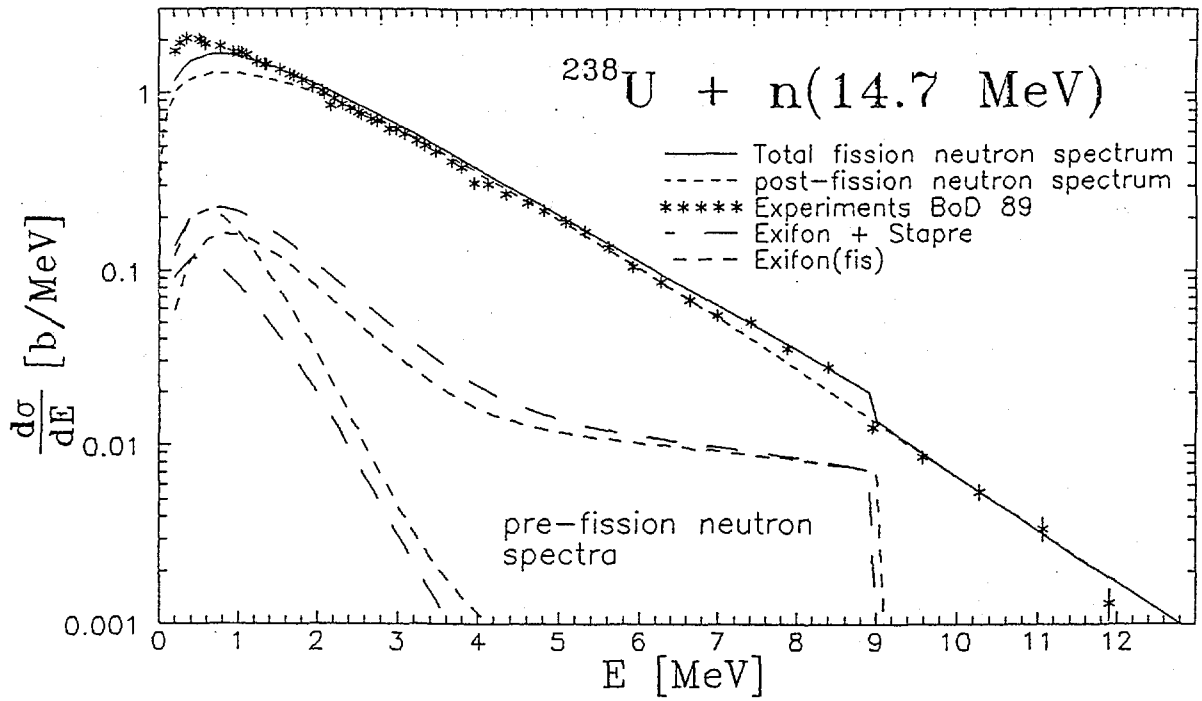

Fig. 21 ^{238}U fission neutron spectrum at 14.7 MeV incidence energy (* - /87/). EXIFON results are presented for two versions: (i) EXIFON including renormalization on the basis of STAPRE partial fission cross sections, (ii) EXIFON with fission channel.

7. SUMMARY

The present review on mechanisms of fission neutron emission started with a brief discussion of dynamical aspects in nuclear fission, since neutron release in fission is strongly connected with the time evolution of the fissioning/scissioning system. Whereas fission neutron observables are well reproduced on the basis of statistical model approaches assuming equilibrium emission from fully accelerated fragments, all possible mechanisms appearing in time scales close to scission point are less understood. At present, it is not possible to draw any definite conclusions about the features of secondary mechanisms, e.g. in quantitative manner. However, several theoretical works discussed in this paper give hints about main characteristics. The representation of the SMA outcomes were mainly based on results obtained at TU Dresden. Nevertheless, the present review gives a general evaluation of experimental and theoretical work in the field.

Clearly, post-fission neutron emission is mainly due to evaporation from fully accelerated fragments. The present status of our knowledge about secondary mechanisms is still crucial.

However, it is justified to consider only equilibrium from fully accelerated fragments in calculations for practical purposes (provided that the main characteristics like the complex fragment occurrence probability are adequately accounted for).

Finally, it is pointed out that any investigations of fission neutron emission mechanisms have to involve sufficient complexity and accuracy in experiment and theory in order to avoid nonreliable conclusions. Any results should be carefully evaluated considering experimental as well as theoretical uncertainties.

References

/ 1/ J. Moreau and K. Heyde, "Theoretical Models of Mass Distributions", Chapter 7 of the "Nuclear Fission Review", ed. C. Wagemans, in press

/ 2/ H. Märten et al., Proc. XVth Int. Conf. on Nuclear Physics - Nuclear Fission, 11 - 15 Nov 1985, ZfK-592 (1986), p. 1

/ 3/ H. Märten, Proc. of the Workshop on Applied Nuclear Theory and Nuclear Model Calculations for Nuclear Technology Applications, Trieste, 15 Feb - 19 Mar 1988, ed. M.K. Mehta and J.J. Schmidt, World Scientific (1989), p. 850

/ 4/ J.M. Blatt and V.F. Weisskopf, Theoretical Nuclear Physics (New York, 1952)

/ 5/ W. Hauser and W. Feshbach, Phys. Rev. 87 (1952) 366

/ 6/ M. Uhl and B. Strohmaier, Report IRK-76/01, IRK Vienna (1976); and Program Manual for STAPRE code, NEA Data Bank (1981)

/ 7/ A.V. Ignatyuk et al., Yad. Fiz. 47 (1988) 355

/ 8/ D.G. Madland and J.R. Nix, Nucl. Sci. Eng. 81 (1982) 213

/ 9/ D. Polster, Proc. XXth Int. Conf. on Nuclear Physics, 12 - 16 Nov 1990, Gaussig near Dresden, in press

/10/ S. Bjornholm and J.E. Lynn, Rev. Mod. Phys. 52 (1980) 725

/11/ J.F. Berger et al., Nucl. Phys. A428 (1984) 23c

/12/ V.M. Strutinsky, Nucl. Phys. A 502 (1989) 67c

/13/ J.W. Negele, Rev. Mod. Phys. 54 (1982) 913

/14/ G.D. Adeev and V.V. Pashkevich, Nucl. Phys. A 502 (1989) 405c

/15/ H.A. Weidenmüller, Nucl. Phys. A 502 (1989) 387c

/16/ K.T.R. Davis et al., Phys. Rev. C 13 (1976) 2385

/17/ J.W. Negele et al., Phys. Rev. C 17 (1978) 1098

/18/ N. Carjan et al., Nucl. Phys. A 452 (1986) 381

/19/ J.R. Nix and A.J. Sierk, Los Alamos National Laboratory Report, LA-UR-87 (1987) 133

/20/ U. Brosa et al., Z. Naturforschung 41A (1986) 1341

/21/ H. Märten, Proc. Int. Conf. on the Fiftieth Anniversary of Nuclear Fission, Leningrad, 16 - 20 Oct 1989, in press; and A. Ruben et al., Z. Phys. A 338 (1991) 67

/22/ B.C. Samanta et al., Phys. Lett. 108B (1982) 83

/23/ H. Märten and D. Seeliger, J. Phys. G10 (1984) 349

/24/ H. Nifenecker et al., Proc. IAEA Symp. on Physics and Chemistry of Fission, Rochester, 13 - 17 Aug 1973 (IAEA, Vienna, 1974) p. 117

/25/ N. Bohr and J.A. Wheeler, Phys. Rev. 56 (1939) 426

/26/ N. Feather, U.S. Atomic Energy Commission, Document BR 335 A (1942), unpublished, cf. Ref. /24/

/27/ B.E. Watt, Phys. Rev. 87 (1952) 1037
/28/ J. Terrell, Phys. Rev. 113 (1959) 527
/29/ R.R. Wilson, Phys. Rev. 72 (1947) 189
/30/ J.S. Fraser, Phys. Rev. 88 (1952) 536
/31/ V.N. Nefedov, J.E.T.F. 38 (1960) 1657
/32/ H.R. Bowman et al., Phys. Rev. 126 (1962) 2120, and Phys. Rev. 129 (1963) 2133
/33/ S.S. Kapoor et al., Phys. Rev. 131 (1963) 283
/34/ K. Skarsvag and K. Bergheim, Nucl. Phys. 45 (1963) 72
/35/ C.P. Sargent et al.,Phys. Rev. B137 (1965) 89
/36/ J.C.D. Milton and J.S. Fraser, Proc. IAEA Symp. on Physics and Chemistry of Fission, Salzburg, 22 - 26 Mar 1965 (IAEA, Vienna, 1965), Vol. II, p. 39
/37/ M.V. Blinov et al., Yad. Fiz. 12 (1970) 41, and Yad. Fiz. 16 (1972) 1155
/38/ C.J. Bishop et al., Nucl. Phys. A 198 (1972) 161
/39/ Z. Fraenkel et al., Phys. Rev. C 12 (1975) 1809
/40/ S. Nair et al., J. Phys. G 3 (1977) 949
/41/ S. Nair et al., J. Phys. G 3 (1977) 965
/42/ V.M. Piksaikin et al., Yad. Fiz. 25 (1977) 723
/43/ Yu.S. Samyatnin et al., Yad. Fiz. 29 (1979) 595
/44/ P. Riehs, Acta Phys. Austr. 53 (1981) 271
/45/ Yu.A. Vasilyev et al., IAEA-Report INDC(CCR)-177/L (1982) 49
/46/ E.A. Seregina et al., Yad. Fiz. 42 (1985) 1337, and Yad. Fiz. 43 (1986) 1092
/47/ C. Budtz-Jorgensen and H.H. Knitter, Radiation Effects 93 (1986) 341
/48/ H. Märten et al., Radiation Effects 93 (1986) 41
/49/ O.I. Batenkov et al., Proc. IAEA Cons. Meeting on Physics of Neutron Emission in Fission, Mito, 24 - 27 May 1988, INDC(NDS)-220/L (IAEA, Vienna, 1989) 207
/50/ H. Märten et al., Proc. Int. Conf. on Nuclear Data for Science and Technology, Mito, 30 May - 3 Jun 1988, ed. S. Igarasi (JAERI, Saikon Publ. Co., Ltd., 1988), p. 683
/51/ C. Budtz-Jorgensen and H.H. Knitter, Nucl. Phys. A 490 (1988) 307
/52/ K. Arnold et al., Nucl. Phys. A 502 (1989) 325c
/53/ A. Gavron, Phys. Rev. C 13 (1976) 2561
/54/ T. Ericson and V.V. Strutinsky, Nucl. Phys. 8 (1958) L 84 (Errata: Nucl Phys. 9 (1959) 689
/55/ K.-H. Schmidt et al., Z. Phys. A 308 (1982) 215
/56/ B. Holmqvist, Arkiv Fysik 38 (1968) 403
/57/ F.D. Becchetti and G.W. Greenlees, Phys. Rev. 182 (1969) 1190
/58/ D. Wilmore and P.E. Hodgson, Nucl. Phys. 55 (1964) 673
/59/ P.A. Moldauer, Nucl. Phys. 47 (1963) 65
/60/ J.C. Browne and F.S. Dietrich, Phys. Rev. C 10 (1974) 2545
/61/ B.F. Gerasimenko and V.A. Rubchenya, Atomnaya Energia 59 (1985) 335
/62/ D. Seeliger et al., loc. cit. /21a/, and INDC(GDR)-056/L (1989)
/63/ H. Märten et al., Proc. Int. Conf. on 50 YEARS WITH NUCLEAR FISSION, Gaithersburg, 25 - 28 April 1989, ed. by J.W. Behrens and A.D. Carlson, ANS (1989), Vol. II, p. 743
/64/ W. Mannhart, Handbook of Nuclear Activation Data, Technical Report Ser. 273 (IAEA, Vienna, 1987) 163
/65/ H. Märten et al., Nucl. Instr. Meth. A 264 (1988) 375
/66/ H. Märten, Proc. Int. Conf. on Physics and Chemistry of Fission, Gaussig near Dresden, 21 - 25 Nov 1988, ed. by H. Märten and D. Seeliger, ZfK-732, p. 155

/67/ U. Brosa et al., Z. Naturforschung 41a (1986) 1341
/68/ U. Brosa, Phys. Rev. C 38 (1988) 1944
/69/ R.W. Hasse and W.D. Myers, Geometrical Relationships of Macroscopic Nuclear Physics, Springer-Verlag (1988) 44
/70/ U. Brosa and H.H. Knitter, loc. cit. /66/, p. 145
/71/ V.S. Stavinsky, J.E.T.P. 36 (1959) 629
/72/ R.W. Fuller, Phys. Rev. 126 (1962) 684
/73/ Y. Boneh and Z. Fraenkel, Phys. Rev. C 10 (1974) 893
/74/ V.A. Rubchenya, preprint RI-28 (Radium Institute Leningrad, 1974)
/75/ P. Mädler, Z. Phys. A 321 (1985) 343
/76/ B. Milek et al., Phys. Rev. C 37 (1988) 1077
/77/ V.P. Eismont, Atomnaya Energia 19 (1965) 113
/78/ G.A. Pik-Pitchak, Yad. Fiz. 10 (1969) 321
/79/ D.J. Hinde et al., Phys. Rev. Lett. 52 (1984) 986
/80/ B.C. Samanta et al., Phys. Lett. 108 B (1982) 83
/81/ H. Märten and D. Seeliger, J. Phys. G 14 (1988) 211
/82/ A. Ruben et al., Z. Phys. A 338 (1991) 67
/83/ H. Kalka et al., Z. Phys. A 329 (1988) 331
/84/ H. Kalka, submitted to Z. Phys. (1991)
/85/ D. Seeliger et al., Yad. Fiz. 47 (1988) 635
/86/ E. Cheifetz et al., Phys. Rev. Lett. 29 (1972) 805
/87/ G.S. Boikov et al., loc. cit. /21/